Development of an array of liquid-scintillator-based bar detectors: SABRE

M. Febbraro[a], D. Walter[b], K.A. Chipps[a,*], S.D. Pain[a], E. Temanson[e,a], R. Toomey[b,g], A. Atencio[b], C.R. Thornsberry[d], K. Smith[d], J. O'Neill[a,d,g], K.L. Jones[d], C.C. Havener[a]

[a]*Physics Division, Oak Ridge National Laboratory, Oak Ridge, TN*
[b]*Department of Physics and Astronomy, Rutgers the State University of New Jersey, Piscataway, NJ*
[c]*Department of Physics, University of Surrey, Guildford, UK*
[d]*Department of Physics and Astronomy, University of Tennessee, Knoxville, TN*
[e]*Physics Department, University of Wisconsin-La Crosse, Lacrosse, WI*
[f]*Physics Department, Tennessee Technological University, Cookeville, TN*
[g]*Physics Department, University of Surrey, Guildford, UK*

Abstract

An array of neutron detectors based on liquid scintillator technology has been developed for nuclear reaction studies, in particular measurements with radioactive ion beams (RIBs). Reaction measurements with RIBs often involve low reaction yields and high gamma-induced backgrounds, which requires high solid angle coverage, high efficiency, and background reduction capability. The kinematics of the reaction neutrons require energy and position determination with good resolution, but preferably without a large number of readouts to minimize cost. To address these requirements, the Scintillation Array of Bars for Reaction Experiments (SABRE) consists of five 12" long, 2" diameter bar detectors filled with organic liquid scintillator and capped at both ends with individually read-out superbialkali photomultiplier tubes (PMTs). In-house purification of the scintillator mixtures resulted in improved light collection. Discussion of the liquid scintillator development and the design and commissioning of SABRE will be presented.

Keywords: Neutron detection; Transfer reactions; Pulse shape discrimination; Radioactive ion beams.

1. Introduction

Neutron detection is an important tool in experimental nuclear physics. Major thrusts in nuclear physics include the evolution of single-particle structure, the limits of nuclear binding, the origin of the heavy elements, and the nuclear matrix elements relevant to neutrinoless double beta decay. In these and many other studies, the spectroscopic detection of neutrons can provide insight: the

---

Corresponding author. E-mail address: kchipps@nuclearemail.org

single-nucleon transfer reaction (d,n) preferentially populates strong proton-single-particle states in unstable nuclei; neutron elastic and inelastic scattering can elucidate the nature of neutron-dense matter such as neutron skins; (α,n) reactions on low-mass seed nuclei emit a large neutron flux in the interiors of Asymptotic Giant Branch stars, driving nucleosynthesis; the charge-exchange (p,n) reaction can provide information on electron capture in supernovae; and (^{3}He,n) proton-pairing reactions on potential $0\nu\beta\beta$ candidates can validate nuclear matrix element calculations. In these example cases as in many others, the reaction of interest must be performed in inverse kinematics with a radioactive ion beam (RIB), which may have low reaction yields, and which compresses the neutron kinematics making position (angular) resolution important. Hence, efficient detection of the energy and interaction point of fast ($\sim$MeV) neutrons emitted in the reaction is crucial, driving a need for position-sensitive, high solid angle, high resolution detectors for neutron spectroscopy.

Various types of neutron detector materials have been employed for fast neutron detection, including plastic scintillators and organic liquid scintillators. These materials do not moderate the neutron energies before detection and therefore may be used for spectroscopy via the neutron time-of-flight (nToF) technique. However, in many cases a continuous background of gammas may be expected, both from natural background sources as well as beam-induced radiation. This extra background cannot be removed using standard time-of-flight techniques, but can be removed using the technique of pulse shape discrimination (PSD) for neutron/γ discrimination. Both standard plastic and liquid scintillator are inexpensive and easy to fabricate, but plastic scintillators have limited neutron/gamma (n/γ) discrimination capability. So-called "PSD plastic," or plastic scintillator designed with PSD capability (for example, [1]), can become prohibitively expensive when used in the large quantities needed for RIB-driven measurements. Organic liquid scintillators, however, exhibit strong inherent n/γ PSD for low-cost standard materials while maintaining time-of-flight capability, and hence were chosen for the design of SABRE. Particularly in the era of radioactive ion beams (RIBs) where production via fragmentation or even the beam itself may produce background gamma rays via decay, pulse shape discrimination is of tremendous use in enabling the next generation of nuclear physics measurements with neutrons.

2

2. Development of SABRE

2.1. Liquid Scintillator Development

Liquid scintillator technology has been utilized in nuclear physics applications for decades; see, for example, Refs. [2–4]. In the current work, effort was made to optimize and purify the scintillator mixtures for the SABRE detectors. While it is possible to use the non-nToF technique of spectrum unfolding with deuterated organic scintillators [5], for cost reasons this technique was not employed for SABRE, and only hydrogenated organic scintillators were considered. A benefit of using liquid scintillators is the ability to easily deploy the scintillator material in detectors of various geometries, allowing the development of the active detection materials to be decoupled from the development of specific detector arrays or implementations.

While liquid scintillator mixtures are available commercially, in-house development provides several benefits. It allows the liquid scintillator formulation (or "cocktail") to be purified to stricter standards, and to be tuned to meet various experimental objectives, such as PSD threshold, light output, ease of handling, or other considerations which might be required for next-generation radioactive ion beam facilities, such as the Facility for Rare Isotope Beams (FRIB). Based on the work of Ref. [3, 4], an initial "standard" liquid scintillator cocktail composed of naphthalene, 2,5-diphenyloxazole (PPO), and 1,4-bis(5-phenyloxazol-2-yl) benzene (POPOP) was produced, with p-xylene as the solvent. The introduction of naphthalene is known to enhance pulse shape discrimination properties [6]. Using a 2" diameter borosilicate glass test cell as shown in Figure 1 coupled to a 2" diameter Hamamatsu superbialkali photomultiplier tube (PMT; Model: R6231-100-01 ASSY), this "standard" mixture was tested and its PSD performance was found to be comparable to several commercially available organic liquid scintillators. Because this initial composition was previously demonstrated in the literature [3, 4] and was similar to what was commercially available, it was used as a reference for the improvements discussed below.

All reagents were acquired through Sigma Aldrich with an initial reported purity of 99% or greater. Scintillation-grade naphthalene and anhydrous p-xylene were used. The p-xylene was further purified in-house by triple distillation into a collection flask containing 4Å molecular sieve, to remove any remaining water left in the solvent. The fluors PPO and POPOP were used without further purification, as their concentrations in the cocktail were very low. It was noted that the scintillation grade naphthalene exhibited a yellow/brown contaminant which severely affected the attenuation length of the scintillator (discussed in more detail later). This contaminant was suc-

3

Figure 1: Photograph of the 2" diameter x 2" length borosilicate glass test cell with purge and septa ports.

cessfully removed by a multi-step purification process, which involved triple recrystallization from methanol followed by sublimation. Figure 2 shows the appearance of naphthalene throughout each stage of the purification process, along with their associated Fourier Transform Infrared (FTIR) spectrograms. While no attempt was made to identify the contaminant compound or compounds, Figure 2 clearly shows a reduction in the broad feature between 9 - 9.5 μm after purification, accompanied by a visible change in the material color. The attenuation length of the scintillator for light at 420 nm increased from 1.2 m using the raw naphthalene material to $\sim$3 m after purification, as determined with small liquid samples and a spectrometer. Scintillator cocktails were prepared using standard Schlenk air-free handling techniques. Transfer of the liquid scintillator between each purification and mixing step, as well as into the detector volume, was performed using cannulation into evacuated and argon-purged flasks. Final transfer of the scintillator to the bar detector was performed using a special 1/4" Swagelok adapter retrofit for a cannula, and the scintillator was bubbled with argon to help remove any remaining contaminants from exposure to air. The reader is directed to Ref. [7] for detailed explanations of the purification techniques used in the current
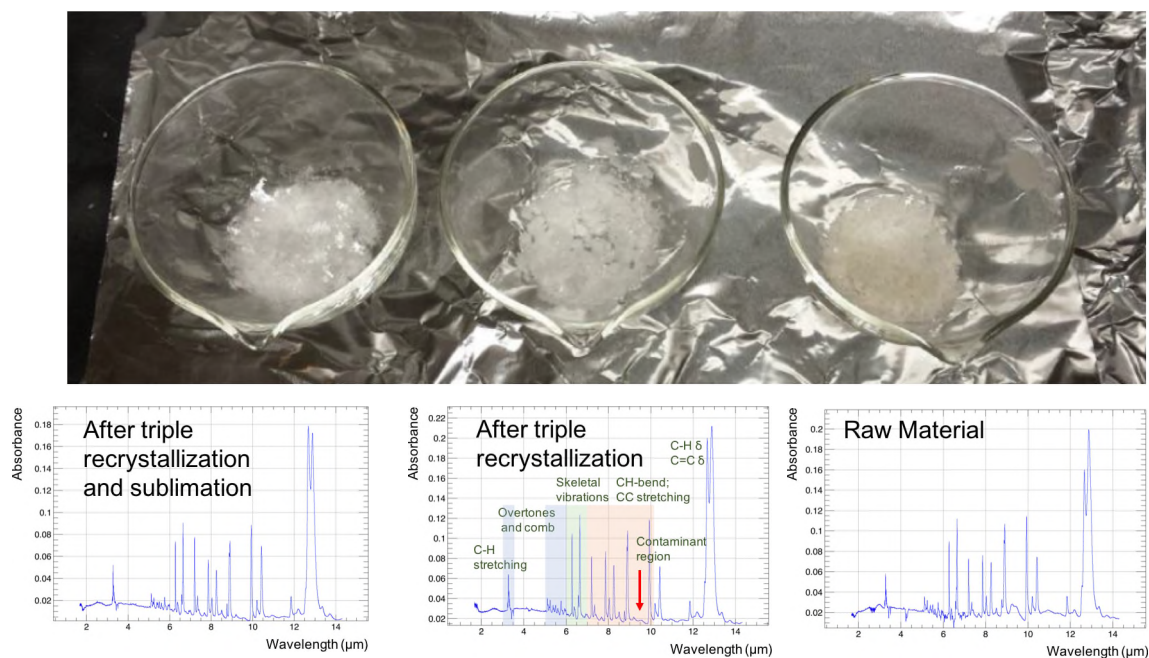
4

Figure 2: Photograph of naphthalene during various stages of purification along with their associated FTIR spectrograms; Initial material (right), after triple recrystallization from methanol (center), and after triple recrystallization and sublimation (left). The middle spectrogram also labels some of the expected spectral structures, for reference.

work. The best-performing cocktail (see Section 3 for a description of the performance) was a mixture of 60 g/L purified naphthalene, 4 g/L PPO, and 0.2 g/L POPOP in purified p-xylene.

Because exposure to air or moisture can cause deterioration to organic liquid scintillators, a small sample of each batch of scintillator cocktail made in-house was kept in a small, air-tight, light-free container labeled with its composition and date. This allowed later comparison between the cocktail as made and the cocktail as it appeared in a SABRE detector, in order to track any potential "aging" or contamination of the scintillator. Throughout the course of the tests described in this paper (cf. Section 3), no noticeable deterioration to the scintillator in the detectors was observed.

2.2. Detector Array Development

The use of scintillator arrays for neutron detection is well established (cf. Ref. [8–11] for example). For the low reaction yields which may be present with radioactive beam measurements, large solid angles need to be covered, necessitating the use of large volumes of neutron detection material. A major disadvantage to the large "neutron wall" type arrays of plastic scintillator bars

5

such as MONA-LISA [12], LENDA [10], and VANDLE [11], when employed for reaction studies with RIBs, is the lack of neutron/gamma discrimination. Such non-PSD plastic scintillator, while simple to fabricate, requires additional external information to suppress the gamma background. Typically, a coincidence detector, usually measuring the beam-like recoil particle, or a timing signal from the accelerator, such as the RF, is required in order to separate neutrons and gammas via time-of-flight. This effectively separates neutrons from prompt gammas, but does not suppress the random background gammas which can dominate over the reaction products of interest by orders of magnitude. Prototype detectors based on PSD plastic, such as PANDORA [13], can be prohibitively expensive when purchased or fabricated in the large volumes needed for RIB reaction measurements. Organic liquid scintillators, on the other hand, provide good n-γ discrimination and can be fabricated in large quantities for relatively modest cost, and hence were chosen for the SABRE bars.

The design of the detectors[1] is based on bars with double-ended light collection, which allows reconstruction of the position of the event inside the detector length. This enables coverage of large solid angles while maintaining spatial sensitivity with minimal electronics channels. This position reconstruction is achievable through either calculation of the difference in arrival time of optical photons between the two ends of the bar, or through the division of collected light (pulse integrals) from the two ends of the bar (*i.e.* light balance or light division), with the integrated light being equated as is standard practice to an electron-equivalent energy (keVee or MeVee). In the case of SABRE, the transit time for light across the bar is short, so without ultrafast timing PMTs, the time difference method for determining position will be less reliable than the light division method, particularly for low light-output events; see Section 3.1 for more details. The bars are 12" in length and 2" in diameter; the diameter takes advantage of inexpensive raw materials and standard PMT sizes, while the length was chosen as a balance between larger detector volume and increased light attenuation.

The bars (see Figure 3) are constructed from 304 stainless steel with a wall thickness of 0.050". The design includes a flange on either end for seating borosilicate glass windows for optical coupling to the PMT, and a single expansion port comprised of a 1/4" tube and Swagelok (compression

---

[1]Throughout the text, imperial units will be used to describe the detectors themselves, as they were designed in inches. Metric units will be used as appropriate for the description of the underlying physics.

fitting) male connector on one end of the bar to displace the inert gas bubble required as an expansion buffer against temperature-induced pressure variations. This is particularly important in the design of liquid scintillator detectors which may be operated with the PMT directly above the optical coupling, as inert gas bubbles inside the detector can drastically diminish the light collection (in many commercial designs, this bubble can account for up to 3% of the detection volume). The expansion port also allows for the bars to be drained and refilled, if a different scintillator cocktail is desired or if the existing cocktail needs to be regenerated. The inner surfaces of the bars were at first electropolished, but tests with this preliminary design demonstrated higher attenuation of the light along the length of the bar than could be tolerated. The second-generation design includes a sleeve of white, polished polytetrafluoroethylene (PTFE) inside of the bar. The windows are 1/8" thick borosilicate glass disks, and a special epoxy (Loctite EA M-31CL Hysol) which is resistant to the xylene solvent is used to adhere the windows in place on the end flanges of the bars.

The individual SABRE detectors have, on each end, a 2" Hamamatsu super-bialkali PMT (R6231-100-01 ASSY), chosen for their low after-pulsing and high resolution. 3D-printed clamps hold the PMTs against the windows on each end of the bar, as well as fastening either a carbon fiber or mu-metal tube around the PMT which provides an optical light-tight seal. Standard optical grease (Saint Gobain BC-630) is used to make the optical coupling between the windows and PMTs. The PMTs are gain matched by adjusting the bias. The array is currently comprised of five double-ended bars, instrumented with a single CAEN V1725 16-channel, 250 MS/s, 14-bit digitizer, controlled via the CAEN WaveDump program [14] through the fiberoptic link. The acquisition can be triggered by individual channels or by requiring a coincidence between both ends of a bar; full, digitized waveforms are read out and stored to a file for later analysis using ROOT [15].

3. Testing and Characterization

3.1. Tests with n/gamma Sources

Comparisons were made between ^{137}Cs source data taken with a SABRE bar containing "stock" liquid scintillator (material that had not been purified after receipt) and the fully-purified liquid scintillator cocktail, as described in Section 2.1. In addition to the attenuation length changes seen with the spectrometer (Section 2.1), the light output of the unpurified bar was 23% less than that from the fully purified bar, based on the measured Compton edge of the source. In addition,
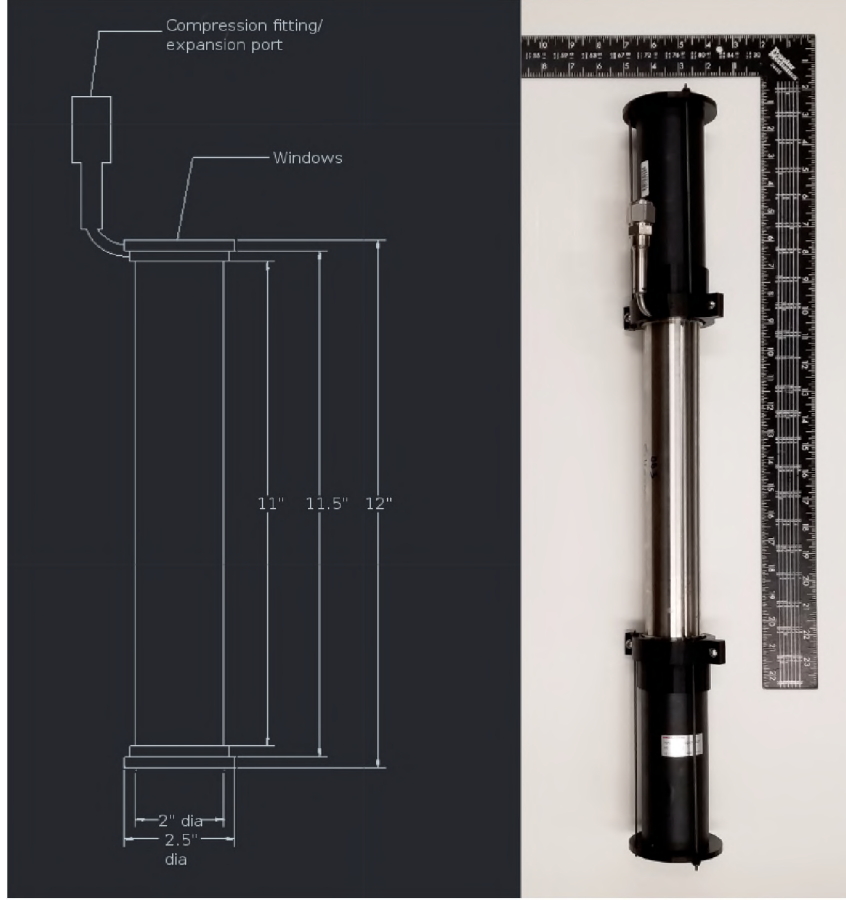
Figure 3: Mechanical line drawing of a SABRE bar, showing some of the important dimensions in inches (not shown is the 0.050" wall thickness), next to a photograph of the latest-generation SABRE bar design, with PMTs mounted.

the figure of merit at 800 keVee (which describes the separation between the neutron and gamma bands in a PSD plot) was roughly 40% higher for the purified cocktail, using a ^{252}Cf n/γ source. Figure 4 shows the PSD response from a SABRE bar with purified scintillator irradiated with ^{252}Cf. Calculation of the PSD parameters from the digitized waveforms with the "tail to total" or "charge comparison" method utilized a long integral of 100ns before peak to 400 ns after peak, and a short integral of 40ns before peak and 400ns after peak.

Position sensitivity measurements based on light balance, defined as:

$$LB = \frac{(\mathscr{L}_{left} - \mathscr{L}_{right})}{(\mathscr{L}_{left} + \mathscr{L}_{right})} \tag{1}$$
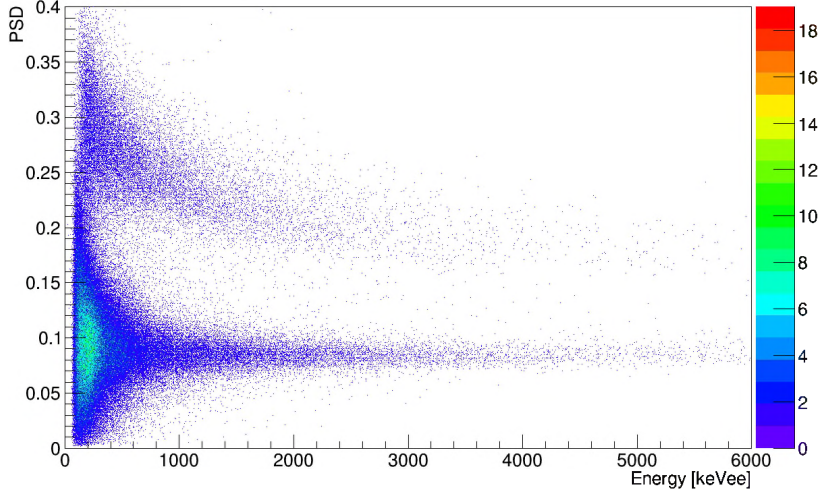
Figure 4: Plot demonstrating the PSD technique for one of the SABRE detectors exposed to an uncollimated ^{252}Cf n-γ source. Calculation of the PSD parameters for this plot utilized a long integral of 100ns before peak to 400 ns after peak, and a short integral of 40ns before peak and 400ns after peak. The figure of merit at 800 keVee for this bar is 1.69.

where $\mathscr{L}$ are the total integrated light yield from each PMT (left or right), were performed for the bar containing fully purified cocktail (as described in Section 2.1) using a $\sim$7 μCi ^{137}Cs source, collimated to 3/16" with 4"x4"x8" tin blocks, placed $\sim$6" away from the bar. Data were taken at eleven positions from -5 to 5 inches along the bar in steps of 1 inch, which allowed for a calibration between light balance (LB) value and physical position of interaction along the bar length. Data were collected at each position for approximately 30 minutes. A light threshold of 100 keVee on each end of the bar was applied in software in the offline analysis. The results are shown in Figure 5.

The position reconstruction based on time difference (right arrival time minus left arrival time, using an optimized half-Gaussian CFD filter algorithm) was also examined for the purified bar for the eleven positions previously discussed, as shown in Figure 6. At the center position, the timing difference resolution was 1.85 ns, corresponding to a position resolution of nearly 3" (σ); this resolution was relatively constant ($<$8%) across the bar, as it is dominated by the PMT with the lesser photon counting statistics, regardless of position. This is significantly worse than the light balance method (cf. Figure 5), and hence the time difference method is not recommended for such short bars with PMTs having a long transit time spread. An independent test of the SABRE
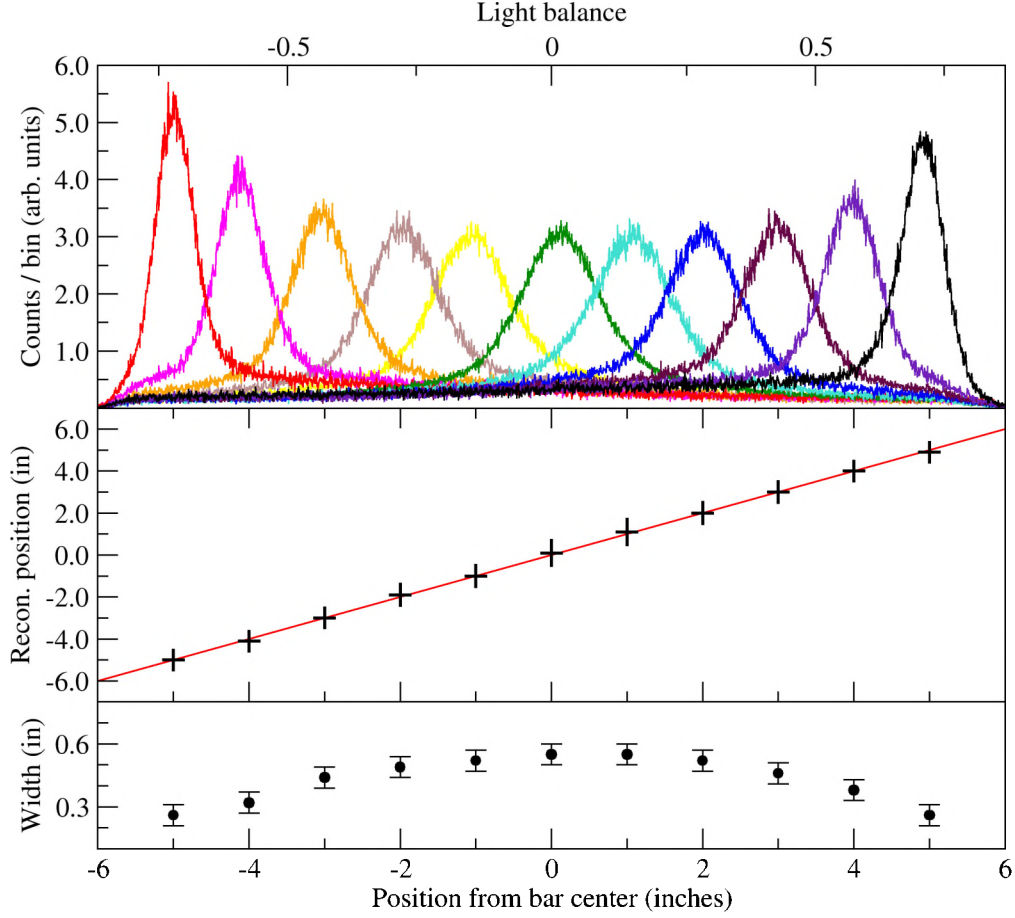
9

Figure 5: Position sensitivity of a SABRE bar with fully-purified naphthalene and distilled xylene to a ^{137}Cs source. Top panel: histogram of the summed light output (left+right) for the 11 different position settings of the collimated source, from left (red) to right (black), as a function of light balance LB (Eq. 1). Middle panel: reconstructed position vs actual position along the bar, from the light balance in the top panel. The vertical bars shown represent $\pm\sigma$ from the light output curves in the top panel. Bottom panel: position resolution (σ) in inches for each source position.

bar timing resolution was performed with the gamma flash from a custom, uncollimated, ∼1 ns timing resolution ^{252}Cf fission chamber [16] placed one foot away from the center of the bar, and again utilizing a half-Gaussian CFD algorithm and 100 keVee threshold. In addition, a software cut on the light balance $LB = 0 \pm \sigma$ (the center of the bar within the measured resolution) was applied, and the broadening contribution from the source was removed in quadrature. This analysis
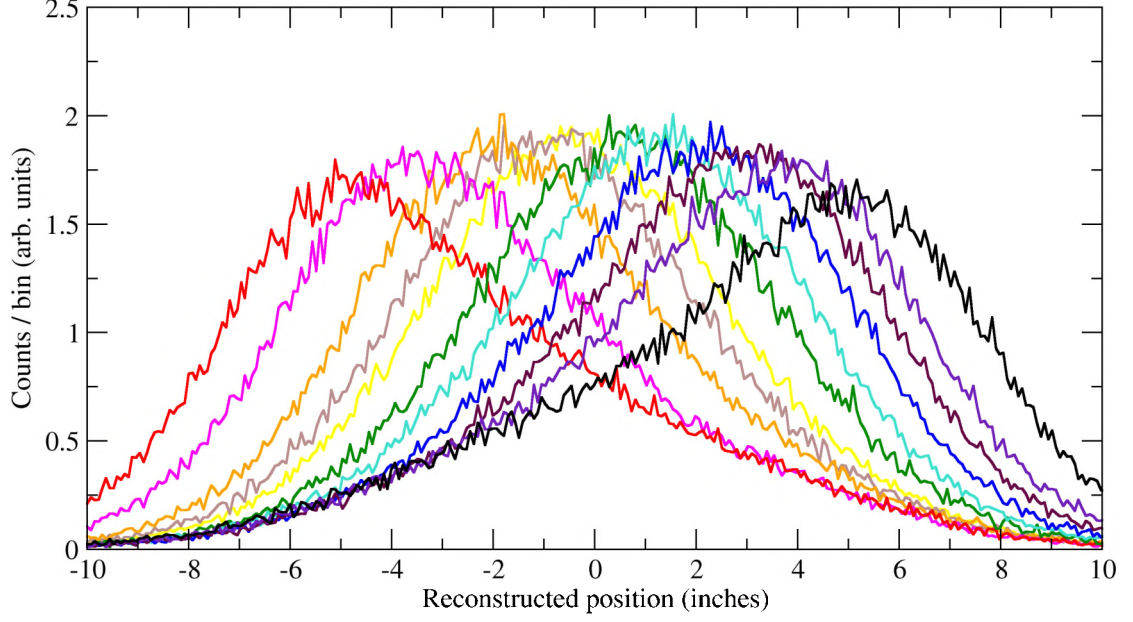
Figure 6: Position sensitivity of a SABRE bar with triple-recrystallized (fully purified) naphthalene to a ^{137}Cs source, using the time difference method to reconstruct the position of interaction along the length of the bar. Cf. the top panel of Figure 5. The digitizer operates at 250 MS/s.

indicates that the timing resolution achievable with the ToF method for these bars and PMTs is on the order of 1.2 ns FWHM (improving to 1.1 ns with a 200 keVee threshold). Faster PMTs will further improve this value, at a cost of higher afterpulsing and/or lower resolution in collected light. It is worth noting, however, that for neutrons under ~10 MeV energy, the transit time of the neutron across the 2" diameter of the bar will dominate over this intrinsic timing resolution.

The complete response of a fully purified bar to a ~6 μCi ^{60}Co source collimated as before in the center (0") source position is shown in Figure 7. The entire bar length is illuminated with an

attenuated γ flux, corresponding to γ rays traversing the collimator material. The light collection as a function of position of interaction in the bar is demonstrated by the Compton edge, which appears as a U shape in Figure 7. This shape is due to the light collection depending on the solid angle subtended by the two PMTs, which in turn depends on the interaction position along the bar. The higher-statistics region in the center is gammas which have passed unimpeded through the $\sim$0.2" collimator, demonstrating the position resolution of the bar.

This position resolution as a function of light (and hence energy) was studied for the fully purified bar using the ^{60}Co source described above, collimated as before in the center (0") source position, and is presented in Figure 8. Data were collected at each position for around one hour. The combined Compton edge of the two gammas was used to calibrate the energy equivalence. The higher energy of the ^{60}Co gammas enables study of the dependence of the position resolution on total light yield, up to approximately 1300 keVee. The measured width of the peaks in the position spectrum has contributions from the intrinsic position resolution of the bar stemming from light collection (1/L), the width of the illuminated area on the bar ($\sim$0.2"), and the range of Compton-scattered electrons in the scintillator material; all three terms were included in the fit to the data. As expected, the position resolution improves with increasing deposited energy, as it is dominated by the photon counting statistics from each PMT, but at higher energies the physical size of the collimated source image and the lateral-scattering range of electrons within the bar begin to dominate. Because the ranges of γ-scattered electrons are considerably longer than for neutron-scattered protons, the position resolution for neutrons is anticipated to be better than what is shown in Figure 8.

The response of SABRE to quasi-monoenergetic neutrons was investigated using the d(d,n) reaction at the Multicharged Ion Research Facility (MIRF) at Oak Ridge National Laboratory [17]. The ECR ion source provided a molecular deuterium beam d_2^+ with an energy of 30 keV/d (60 keV total energy) and beam current of about 10 $e\mu A$, which was impinged on a stainless steel flange. As deuterium built up on the target from implanted, unreacted beam, $\sim$2.2 MeV neutrons were generated by the reaction of the deuterium beam with the deuterium self-implantations, at a rate of about 1 kHz in one SABRE bar placed $\sim$4" away. Figure 9 shows the performance of a SABRE bar to the $\sim$2.2 MeV neutrons using the charge integration or "tail to total" method for PSD.
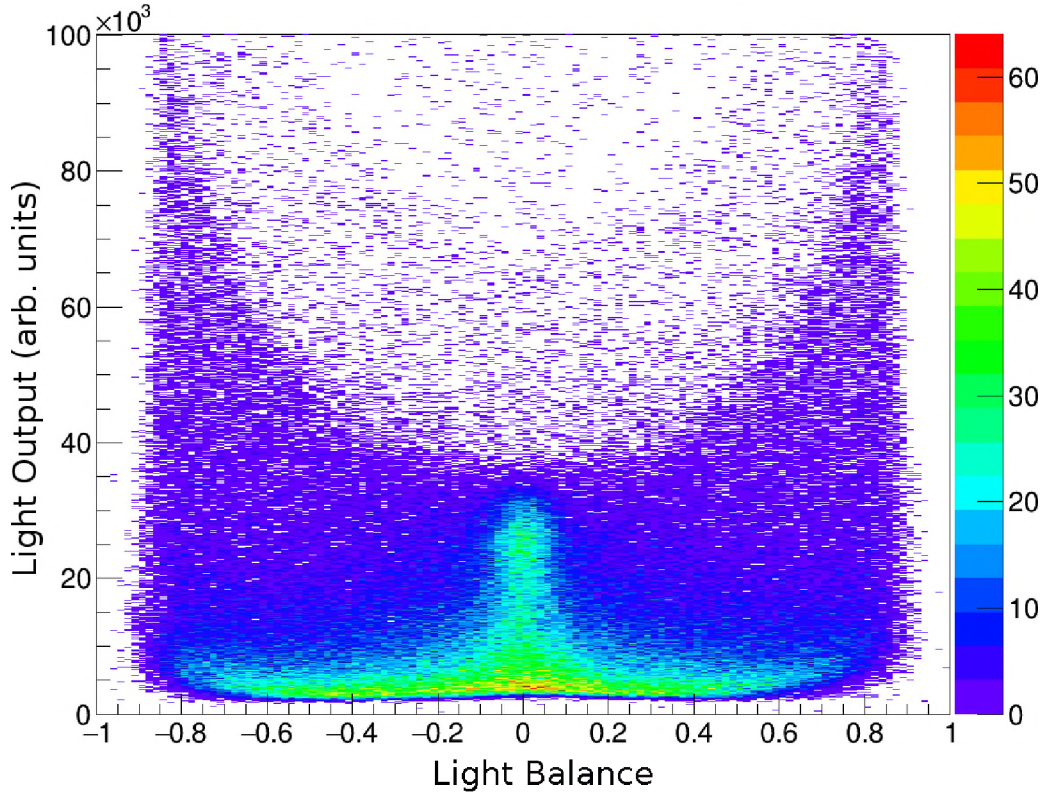
Figure 7: Plot of summed light output (left+right, arbitrary units) of a SABRE bar with fully purified cocktail as a function of light balance LB (Eq. 1) for the ^{60}Co source in the center position, demonstrating the light collection as a function of interaction position along the length of the bar. The area of direct illumination by the source is apparent in the high-statistics peak-like shape in the center location. The Compton edge of the source, visible via attenuated gammas from the source which have passed through the collimator material, is apparent in a U-shape across the entire bar, due to the changing solid angle of each PMT as a function of distance. A light threshold of 100 keVee was applied.

3.2. In-Beam Tests

As an example of the use of SABRE for a neutron spectroscopic measurement, the d(^{12}C,n)^{13}N reaction was studied at the University of Notre Dame's Nuclear Science Laboratory. A ^{12}C beam from the FN tandem impinged on a deuterated polyethylene (C$_2$D$_4$) foil inside of a small scattering chamber. Neutrons from the (d,n) reactions were measured in both the SABRE detectors as arrayed in Figure 10 and a selection of VANDLE [11] detectors covering additional angles. The results of the measurement will be presented in a separate publication [18]. The response of a SABRE bar to the resultant reactions, including a gamma flash and delayed neutron arrival, is shown in Figure
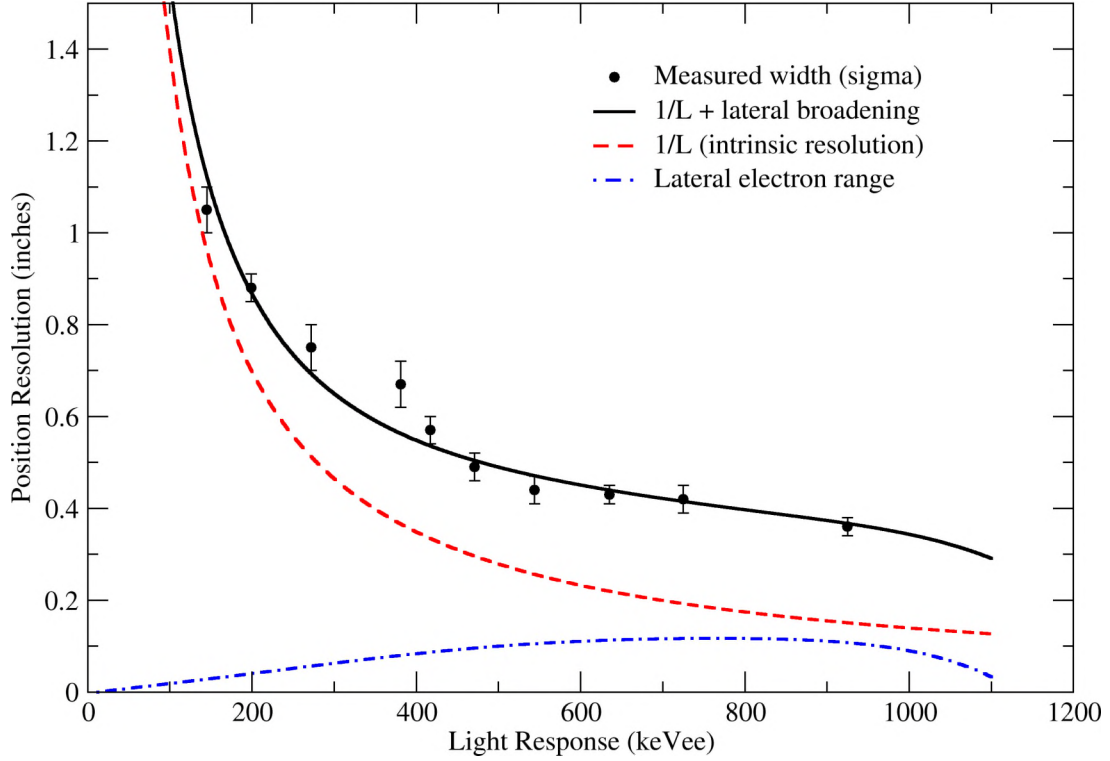
13

Figure 8: Position resolution in inches (σ) of a SABRE bar with fully purified cocktail, as a function of the summed light output (left+right), derived from a ^{60}Co planar source. Uncertainties are from the fit to the light peak. The expected 1/L shape is convolved with a calculation of the broadening effect of the lateral (along the length of the bar) range of Compton-scattered electrons from the ^{60}Co gammas as well as the finite width of the source image.

11. It is apparent that the PSD capability of the SABRE bars allows for significant reduction of gamma background in the neutron spectrum.

As an example of the use of SABRE detectors for a cross section measurement, the ^{13}C(α,n)^{16}O reaction was studied at the Multicharged Ion Research Facility's ion source at Oak Ridge National Laboratory [19]. Figure 12 shows the "barrel" setup used for this quasi-spectroscopic counting measurement (no time-of-flight was possible during this measurement due to the intense DC α
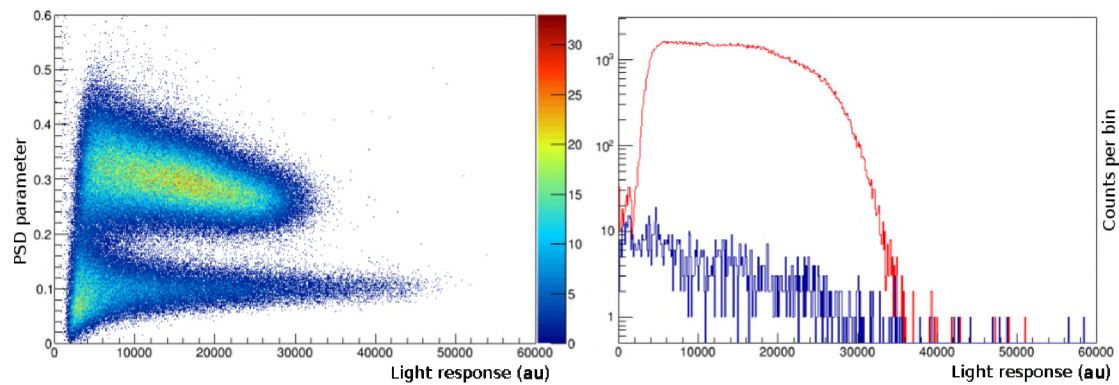
14

Figure 9: PSD plots of the bar detector to ∼2.2 MeV neutrons produced from the d(d,n) reaction (left). A neutron-gated light response spectrum (right), for "beam on" (red) and "beam off" (blue). Light output is in arbitrary units.

Figure 10: Photograph of the SABRE detectors set up in a neutron spectroscopy configuration at the Nuclear Science Laboratory at the University of Notre Dame, for a neutron spectroscopic measurement. The Swagelok expansion port is just visible at the top of each bar, demonstrating how the design protects against light loss due to any expansion bubble.

beam). Neutrons from the reaction of interest had a maximum energy of just over ∼2 MeV, allowing for a quasi-spectroscopic energy cut to be made on the PSD plot, effectively discriminating against gammas and suppressing higher-energy neutrons from other reactions, as is shown in Figure 13.
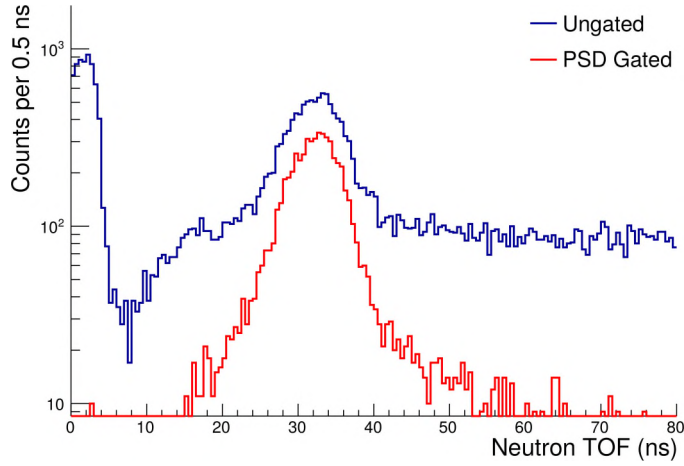
15

Figure 11: Time-of-flight response of a SABRE bar to the $d(^{12}C,n)$ reaction. The blue curve is all events, and the red curve is with the PSD gate applied. Removal of the gamma flash, inherent to all time-of-flight neutron measurements, as well as the random gamma background across the entire TOF spectrum, is apparent.
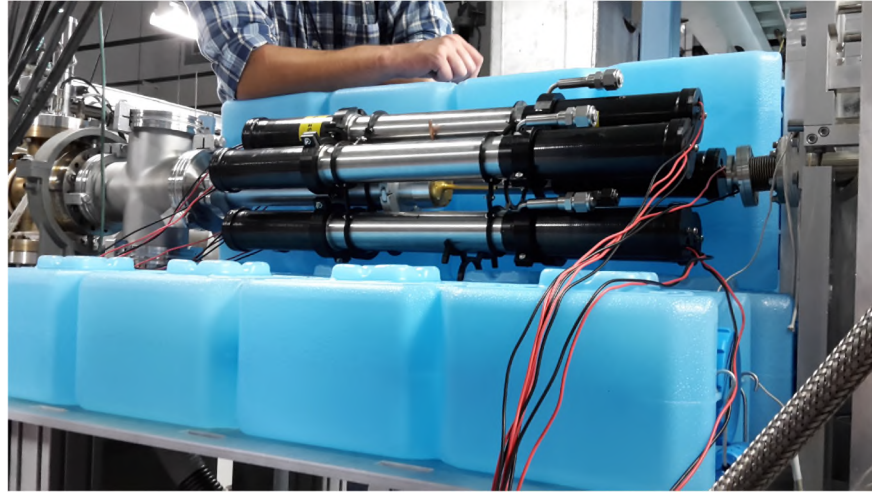

Figure 12: Photograph of the SABRE detectors set up in a barrel configuration around the target location at the Multicharged Ion Research Facility (MIRF) at Oak Ridge National Laboratory, for a cross section (counting) measurement. The blue water bricks used as shielding can be seen in the background.

4. Summary

The preliminary SABRE implementation includes five bar detectors with Hamamatsu super-bialkali PMTs and a single 16-channel CAEN digitizer module controlled through the optical link.
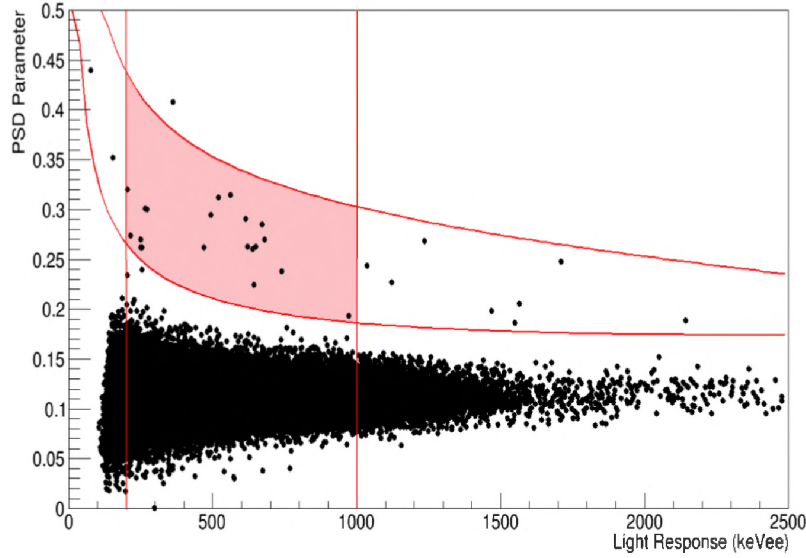
16

Figure 13: PSD plot from one of the SABRE detectors during the ^{13}C$(\alpha,\text{n})^{16}$O reaction study at MIRF, demonstrating the region of interest. Adapted from Ref. [19].

This implementation has been used successfully in experiments at both the University of Notre Dame's Nuclear Science Laboratory and the Multicharged Ion Research Facility at Oak Ridge National Laboratory. The organic liquid scintillator mixtures used in the SABRE detectors were purified and characterized, and can be tailored to specific experimental requirements. An expansion of the array is planned, both in number of detectors and in consideration of alternative geometries optimized to solid angle coverage at very forward and backward laboratory angles, in order to facilitate future large-scale reaction measurements with radioactive ion beams.

5. Acknowledgments

17

of Nuclear Physics, under contract number DE-AC05-00OR22725.

References

[1] Eljen Technologies, EJ-276 PSD Plastic Scintillator, Date accessed 13 April 2018.
URL http://eljentechnology.com/products/plastic-scintillators/ej-276

[2] I. Berlman, O. Steingraber, Liquid scintillation solutions for pulse-shape discrimination, Nuclear Instruments and Methods 108 (3) (1973) 587 – 591. doi:http://dx.doi.org/10.1016/0029-554X(73)90542-9.
URL http://www.sciencedirect.com/science/article/pii/0029554X73905429

[3] D. L. Horrocks, Scintillation efficiencies at high solute concentrations: Possible energy transfer from s3 states of excited aromatic solvents, The Journal of Chemical Physics 52 (3) (1970) 1566–1572. doi:10.1063/1.1673168.
URL http://dx.doi.org/10.1063/1.1673168

[4] J. Birks, G. Poullis, Liquid scintillators, in: M.A. Crook, P. Johnson, B. Scales (Ed.), Liquid Scintillation Counting: Proceedings of a Symposium on Liquid Scintillation Counting organized by the Society for Analytical Chemistry, Vol. 2, Heyden & Son Ltd, 1971, p. 1.

[5] M. Febbraro, PhD thesis, Ph.D. thesis, University of Michigan (2014).

[6] V. Verbinski, W. Burrus, T. Love, W. Zobel, N. Hill, R. Textor, Calibration of an organic scintillator for neutron spectrometry, Nuclear Instruments and Methods 65 (1) (1968) 8 – 25. doi:http://dx.doi.org/10.1016/0029-554X(68)90003-7.
URL http://www.sciencedirect.com/science/article/pii/0029554X68900037

[7] W.L.F. Armarego, Purification of Laboratory Chemicals, 8th Edition, Butterworth-Heinemann, 2017.

[8] P. Zecher, A. Galonsky, J. Kruse, S. Gaff, J. Ottarson, J. Wang, F. Dek, . Horvth, . Kiss, Z. Seres, K. Ieki, Y. Iwata, H. Schelin, A large-area, position-sensitive neutron detector with neutron/γ-ray discrimination capabilities, Nuclear Instruments and Methods in Physics Research Section A: Accelerators, Spectrometers, Detectors and Associated Equipment 401 (2) (1997) 329 – 344. doi:http://dx.doi.org/10.1016/S0168-9002(97)00942-X.
URL http://www.sciencedirect.com/science/article/pii/S016890029700942X

18

[9] C. Zhang, D.-M. Mei, P. Davis, B. Woltman, F. Gray, Measuring fast neutrons with large liquid scintillation detector for ultra-low background experiments, Nuclear Instruments and Methods in Physics Research Section A: Accelerators, Spectrometers, Detectors and Associated Equipment 729 (2013) 138 – 146. doi:http://dx.doi.org/10.1016/j.nima.2013.07.012.
URL http://www.sciencedirect.com/science/article/pii/S0168900213009881

[10] G. Perdikakis, S. Austin, D. Bazin, C. Caesar, J. Deaven, C. Guess, G. Hitt, R. Meharchand, D. Nguyen, Y. Shimbara, K. Thorne, R. Zegers, LENDA: A low energy neutron detector array for studies of (p,n) reactions with radioactive beams, IEEE Transactions on Nuclear Science 56 (3) (2009) 1174–1178. doi:10.1109/TNS.2009.2014847.

[11] W. Peters, S. Ilyushkin, M. Madurga, C. Matei, S. Paulauskas, R. Grzywacz, D. Bardayan, C. Brune, J. Allen, J. Allen, Z. Bergstrom, J. Blackmon, N. Brewer, J. Cizewski, P. Copp, M. Howard, R. Ikeyama, R. Kozub, B. Manning, T. Massey, M. Matos, E. Merino, P. O'Malley, F. Raiola, C. Reingold, F. Sarazin, I. Spassova, S. Taylor, D. Walter, Performance of the Versatile Array of Neutron Detectors at Low Energy (VANDLE), Nuclear Instruments and Methods in Physics Research Section A: Accelerators, Spectrometers, Detectors and Associated Equipment 836 (2016) 122 – 133. doi:https://doi.org/10.1016/j.nima.2016.08.054.
URL http://www.sciencedirect.com/science/article/pii/S0168900216308816

[12] N. Frank, T. Baumann, D. Bazin, J. Brown, P. A. DeYoung, J. E. Finck, A. Gade, J. Hinnefeld, R. Howes, J. Lecouey, B. Luther, W. A. Peters, H. Scheit, A. Schiller, M. Thoennessen, Exploring Neutron-Rich Oxygen Isotopes with MoNA, AIP Conference Proceedings 961 (1) (2007) 143–148. doi:10.1063/1.2827247.

[13] L. Stuhl, M. Sasano, K. Yako, J. Yasuda, H. Baba, S. Ota, T. Uesaka, Pandora, a large volume low-energy neutron detector with real-time neutrongamma discrimination, Nuclear Instruments and Methods in Physics Research Section A: Accelerators, Spectrometers, Detectors and Associated Equipment 866 (2017) 164 – 171. doi:https://doi.org/10.1016/j.nima.2017.06.015.
URL http://www.sciencedirect.com/science/article/pii/S0168900217306630

[14] CAEN WaveDump digitizer readout application, CAEN S.p.A., Date accessed 13 April 2018.
URL http://www.caen.it/csite/CaenProd.jsp?parent=38&idmod=692

19

[15] Rene Brun and Fons Rademakers, ROOT - An Object Oriented Data Analysis Framework, Proceedings AIHENP'96 Workshop, Lausanne, Sep. 1996, Nucl. Inst. and Meth. in Phys. Res. A 389 (1997) 81–86, Date accessed 13 April 2018.
URL https://root.cern.ch/

[16] P. Hausladen, private communication.

[17] F. Meyer, M. Bannister, D. Dowling, J. Hale, C. Havener, J. Johnson, R. Juras, H. Krause, A. Mendez, J. Sinclair, A. Tatum, C. Vane, E. B. Musafiri, M. Fogle, R. Rejoub, L. Vergara, D. Hitz, M. Delaunay, A. Girard, L. Guillemet, J. Chartier, The ornl multicharged ion research facility upgrade project, Nuclear Instruments and Methods in Physics Research Section B: Beam Interactions with Materials and Atoms 242 (1) (2006) 71–78, ion Beam Modification of Materials. doi:http://dx.doi.org/10.1016/j.nimb.2005.08.176.
URL http://www.sciencedirect.com/science/article/pii/S0168583X05014722

[18] C. Thornsberry, PhD thesis, Ph.D. thesis, University of Tennessee Knoxville (2018).

[19] R. Toomey, A Low Energy Measurement of the Cross Section of the $^{13}C(\alpha,n)^{17}O$ Reaction (MPhys dissertation), Master's thesis, University of Surrey (2017).